

Mechanical properties and structure of *Strombus gigas*, *Tridacna gigas*, and *Haliotis rufescens* sea shells: A comparative study

Albert Yu Min Lin*, Marc André Meyers, Kenneth S. Vecchio

Department of Mechanical and Aerospace Engineering, Materials Science and Engineering Program, University of California San Diego,
La Jolla, CA 92093-0411, USA

Available online 28 October 2005

Abstract

Sea shells are composed of calcium carbonate crystals interleaved with layers of viscoelastic proteins, having dense, tailored structures that yield excellent mechanical properties. Shells such as conch (*Strombus gigas*), giant clam (*Tridacna gigas*), and red abalone (*Haliotis rufescens*) have hierarchical architectures that differ depending on growth requirements and shell formation of the particular mollusk. Mechanical tests have been carried out on these shells for a comparison of strength with respect to the microstructural architecture and sample orientation. The mechanical response is found to vary significantly from specimen to specimen and requires the application of Weibull statistics in order to be quantitatively evaluated. The complex micro-laminate structure of these biocomposite materials is characterized and related to their mechanical properties. The red abalone has the highest compressive (233–540 MPa) and flexure strengths of the three shells. The giant clam has the lowest strength (87–123 MPa) and the conch has an intermediate value (166–218 MPa) in compression. The high compressive strength observed in the abalone is attributed to an optimization of microstructural architecture in the form of 2-D laminates, enhancing the fracture toughness of this shell material and enabling higher stresses to develop before fracture.

© 2005 Elsevier B.V. All rights reserved.

Keywords: Biological materials; Biomimetics; Abalone; Conch; Giant clam; Mechanical properties

1. Introduction

Natural selection provides a tool by which nature can process, improve, and refine biologically based organisms over millions of years. Scientists can learn from these evolutionary refinements and develop technologies based on natural designs. At present, even the simplest bio-mineralized structures cannot be synthesized in the laboratory without the use of living organisms. This study is done with the intention to contribute to the ongoing development of the next generation of synthetic materials [1,2], based on biomimicry.

Basic inorganic materials used in nature (such as calcium carbonate, hydroxyapatite, and amorphous silicas) are, on their own, very weak. However, when combined with proteins, self-organized into highly ordered structures, and refined over long periods, these basic materials make very strong composites, sometimes increasing their strength by

orders of magnitude [3,4]. Examples of such biological materials include bone, teeth, sponge spicules, diatoms, and mollusk shells [3,5,6]. These complex composites contain both inorganic and organic components in their macro-, micro-, and nanostructures [7,8]. The complexity of these structures and their ability to self-assemble has drawn considerable attention [e.g. Refs.1,9,10]. An increase in strength due to structure can be seen in other laminates as they form stronger materials from weak base materials, however, the relative strength gain found in these biocomposites remains unparalleled in synthetic materials.

By investigating various shells with similar composition, but dissimilar structural organization, one can observe the role of macro-, micro-, and nanostructures in the mechanical response of such biocomposites. The structure and mechanical response of the pink conch (*Strombus gigas*) [6], the giant clam (*Tridacna gigas*), and the red abalone (*Haliotis rufescens*) [1,11,12] are investigated to gain insight on various organized structures that have been developed in nature, with the eventual goal of mimicking them in the synthesis of novel stronger materials [1,2].

* Corresponding author.

E-mail address: a5lin@ucsd.edu (A.Y.M. Lin).

2. Structure

This investigation examines three systems with varying structural complexity. Each animal uses the same base material, CaCO_3 , that is very abundant in nature and creates a composite material, which is on average, over 95 wt.% CaCO_3 and less than 5 wt.% organic protein.

2.1. Conch shell

The conch (*S. gigas*) shell, known for its logarithmic spiral shape, exhibits the highest level of organization in structure among the three shells described. Conch shells have a cross-lamellar structure consisting of lath-like aragonite crystals (99.9 wt.% of the shell) and an organic matrix (0.1 wt.% of the shell) [13]. As presented in Fig. 1, the lath-like aragonite crystals form ‘plywood’-like structures composed of three macro-layers (outer, middle and inner). Each macro-layer is composed of first-order lamellae, which are in turn, formed from second-order lamella, which are further divided into third-order lamellae.

This investigation is focused on the mechanical response of the middle macro-layer, yet it is important to note that the combination of all three layers is responsible for the total mechanical response of the shell. The middle macro-layer shows parallel alignment of first-order lamellae, which are composed of many single-crystal tiles (approximately $10\ \mu\text{m}$ thick \times $150\ \mu\text{m}$ wide) that are stacked upon each other, creating second-order lamellae. The orientation of the tiles differs between rows of the second-order lamella in an alternating pattern of approximately $\pm 35^\circ$ – 45° rotations. The organic matrix has only been observed in TEM as an electron dense layer around each of the individual tiles [14].

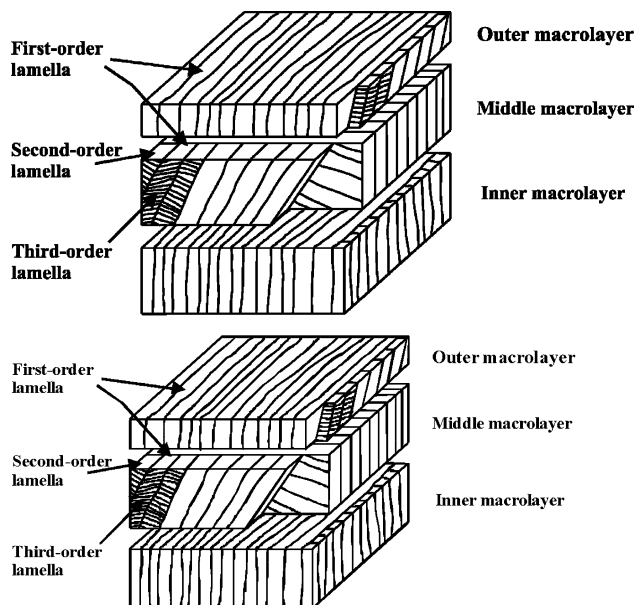


Fig. 1. Schematic drawing of the cross-lamellar structure of *S. gigas*. Each layer also consists of first-, second-, and third-order lamella.

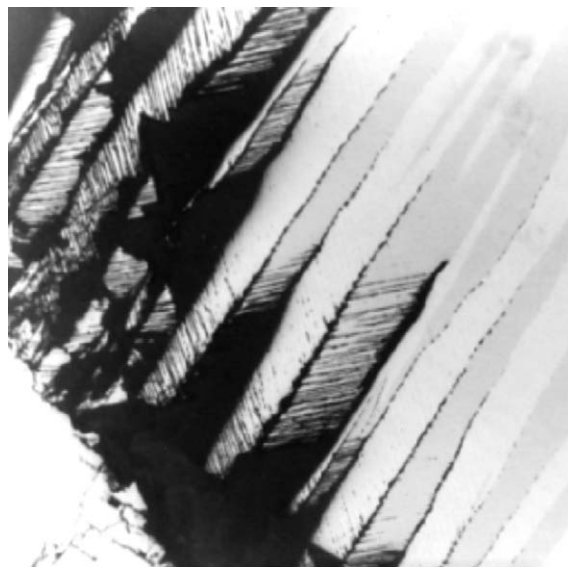


Fig. 2. Middle macro-layer of *S. gigas* shell.

A SEM image of the middle macro-layer of the conch shell is presented in Fig. 2.

2.2. Giant clam shell

The giant clam (*T. gigas*) can grow its shell to widths greater than 1 m, with weights of over 340 kg [15]. The large amount of shell material produced has made the giant clam of interest in both contemporary as well as historical context. There has been documented use of this shell as the raw material for applications such as blades for wood-cutting tools by ancient and present day Takuu Atoll dwellers of Papua New Guinea [16]. The structure of the shell has the lowest level of organization of the three materials in this investigation, yet its sheer mass results in a strong overall system. The protective shell consists of two distinct regions, an outer white region and an inner translucent region.

The outer region acts as the animal's first line of defense against the harsh environment. This region appears to comprise approximately one-third of the shell thickness and is formed from dense structured layers of aragonite needles approximately 1 – $5\ \mu\text{m}$ in length [16]. Growth bands, which extend perpendicular to the direction of shell growth, are thought to contain a thin organic matrix, partially separating layers of cross-lamellar aragonite needles [17]. The structure of the outer region of the shell, presented in Fig. 3, somewhat resembles the microstructure of the middle macro-layer of conch shell, yet a considerable decrease in organization is observed. Growth bands form first-order lamellae, separating layers of second- and third-order lamellae perpendicular to the direction of growth. The second-order lamella is composed of planes, parallel to the growth direction, which separate planes of needles (third-order lamella) with alternating orientation. The directions of needles alternate between $+60^\circ$ and -60° to the direction of growth for each second-order lamella.

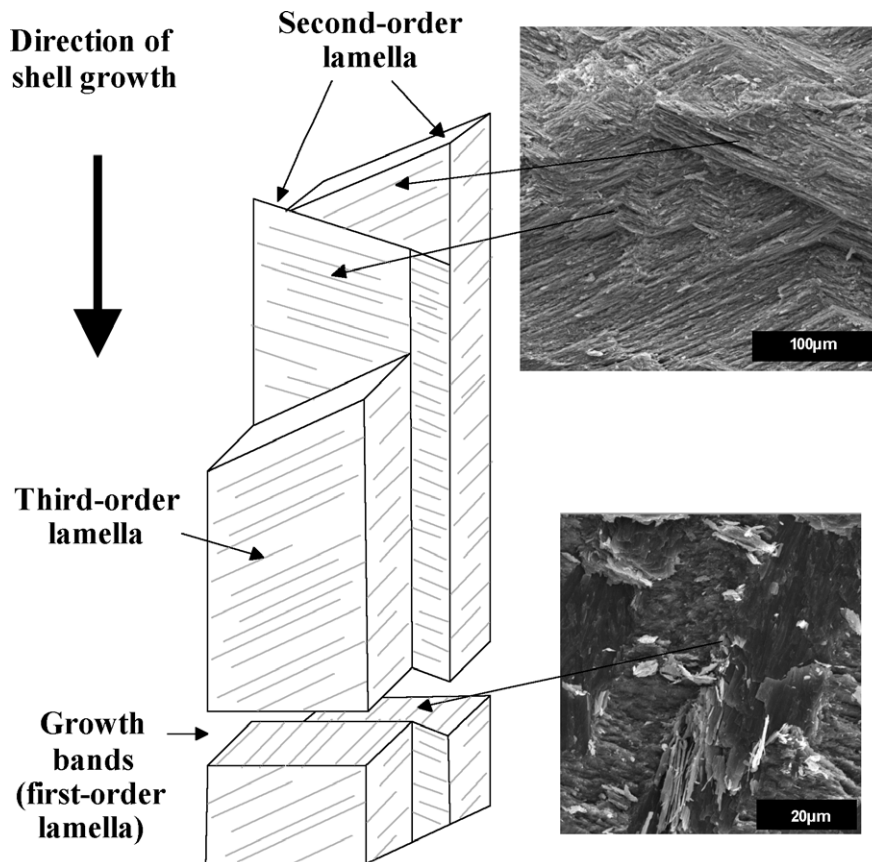


Fig. 3. Schematic representation and SEM image of *T. gigas* shell outer region.

Within the inner region of the shell, the micro-layered structure is also observed as continuous planes of growth bands. These layers separate approximately 3–7 μm of inorganic material and span normal to the direction of shell growth. Long single crystals of aragonite travel along the direction of growth and are not interrupted by growth bands. This inner region appears more transparent than the outer region and contains a high concentration of flaws traveling along the single columnar crystal interfaces. These flaws, in the form of microcracks, travel along the direction of growth facilitating crack propagation along abutting interfaces of neighboring crystals. Fig. 4 shows an optical micrograph of

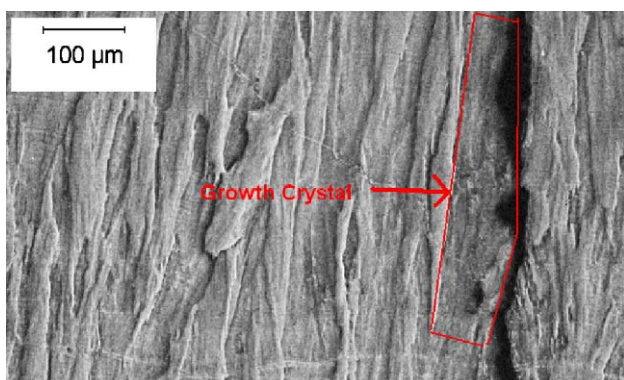


Fig. 4. Optical microscopy of polished cross-sectional specimen of *T. gigas* shell (inner region), with continuous single crystal facilitating crack propagation.

the microcracks along columnar crystal interfaces. The observed growth bands in the microstructure do not interrupt the growth of single crystals from one band to the next and thus have a minimal effect on crack deflection.

2.3. Red abalone shell

The structure of nacre taken from the red abalone (*H. rufescens*) has been well studied as a model system in the growing field of biomimetic and bio-inspired materials. It is the focus of much attention for its exceptional strength, among the highest in shell structures [19], but more importantly for its low (4:1) ratio between compressive strength and tensile strength, uncharacteristic of most ceramics. This ceramic/organic composite is composed of approximately 95 wt.% CaCO_3 and 5 wt.% organic matrix. Similar to the conch and the giant clam, there is both macrostructural and microstructural organization throughout the shell. Fig. 5(a) provides a macrostructural view of a cross-section of the inner nacreous layer and outer calcitic layer of shell. Mesolayers separating larger regions of nacre (approximately 300 μm thick) have been observed by Menig et al. [18]. These “mesolayers” mark interruptions in nacre growth and are believed to be a result of variations in feeding patterns. They are therefore also called growth bands. These interruptions contain large regions of organic matrix between regions of inorganic CaCO_3 which have undergone changes in morphology [18,20]. Fig. 5(b) and (c) show SEM

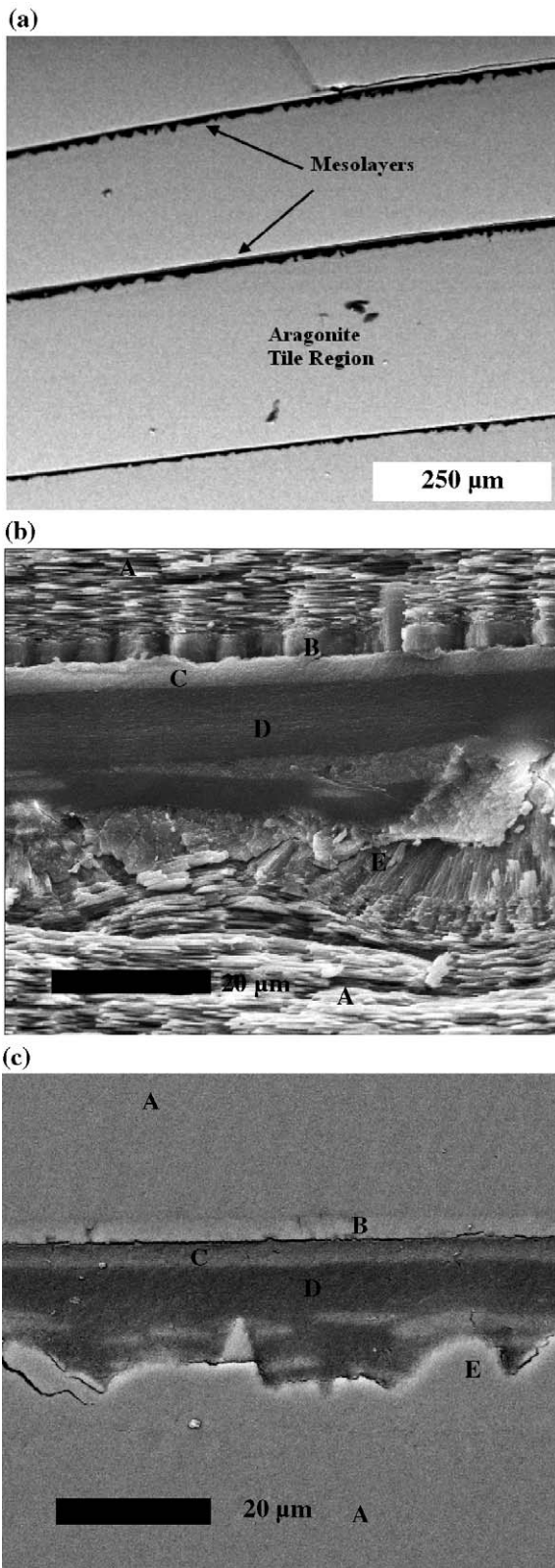


Fig. 5. (a) Macrostructural view of a cross-section of the *H. rufescens* shell. Growth bands are observed separating larger regions of nacre. (b) SEM micrograph of fracture surface and (c) polished surface of mesolayers. Tiles (A); block-like calcite (B); organic/inorganic mix (C); organic (D); and spherulites (E) are observed.

micrographs of a fracture surface and polished surface in abalone, respectively. Five regions can be identified: tiled (A); block-like calcite (B); organic/inorganic mix (C); organic (D); and spherulitic (E). The growth sequence is described in greater detail by Lin and Meyers et al. [20]. In Fig. 5, the growth occurs from top to bottom. Prior to arrest of growth, the characteristic tiles are replaced by a block-like structure (B). This is followed by the massive deposition of the organic layer, which is initially intermediated with mineralized regions. At the end of the mesolayer, when mineralization starts again, a layer comprised of spherulitic features is observed. This layer has been previously identified by, e.g. Zaremba et al. [21]. Adjacent spherulites eventually form, creating a continuous layer. At this juncture, tiles formation reoccurs. This spherulitic layer, which was thought to be calcite, has been recently identified by Su et al. [22] as aragonite. The nanoindentation of tiled aragonite (3.2 GPa) and organic mesolayer (0.56 GPa) confirms the differences. However, it can be concluded that the organic layer is quite stiff (established yield stress ≈ 190 MPa) and is likely to have a much higher mechanical strength than the organic nanolayers between tiles. Once growth is periodically arrested, a 100- μm thick organic layer is produced. Prior to tile growth, a layer starting with columnar aragonite radiating from nucleation sites is produced. After this transitional layer is formed, regular tile

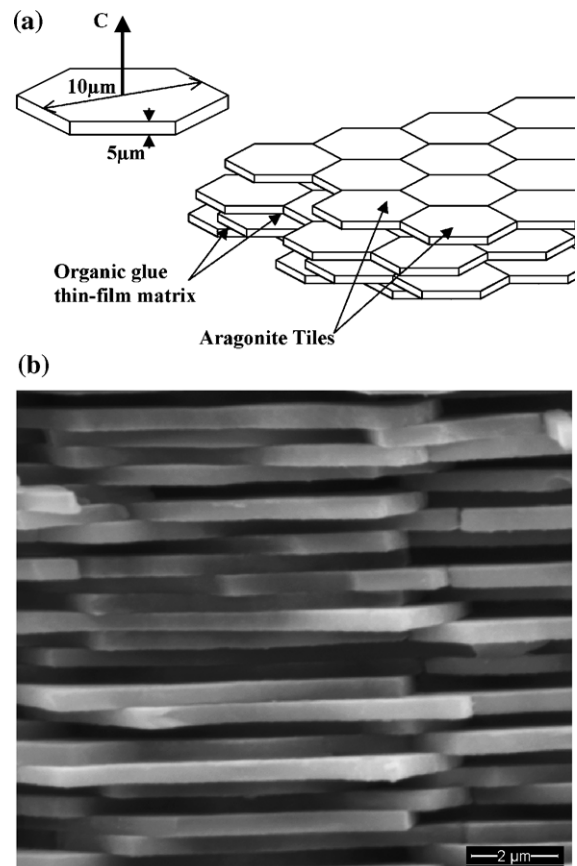


Fig. 6. (a) Schematic representation of microstructure in *H. rufescens*. (b) SEM image of *H. rufescens* microstructure.

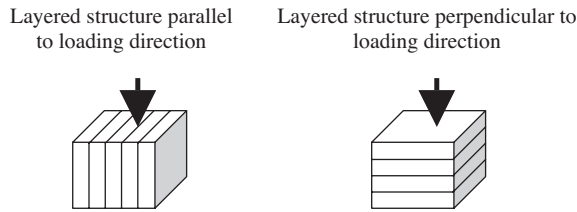


Fig. 7. Loading directions which correspond to labeled curves in Weibull plots.

growth takes place. Menig et al. [18] observed crack deflection at these thick (20 μm) organic interfaces.

The microstructure of the abalone shell is represented in Fig. 6(a) and (b). This region is composed of stacked sheets of pseudo-hexagonal aragonite platelets, which are separated by a thin sheet of organic matrix serving as viscoelastic glue between layers [23,24]. These platelets are characterized by nearly perfect *c*-axis alignment normal to the plane of the tiles. Each tile is approximately 0.5 μm thick, while the thin organic matrix is approximately 20–30 nm thick. Sarikaya et al. [11,12] and Menig et al. [18] proposed several toughening mechanisms within this region: (a) crack blunting/branching/deflection, (b) the formation of microcracks, and (c) plate pullout between layers of tile and sliding of entire platelet planes.

3. Experiment procedures

3.1. Mechanical testing

3.1.1. Compression

Samples of each shell were tested in compression both parallel and perpendicular to shell growth bands under quasi-static and dynamic strain rates. It should be noted that, as described in Section 2, each of the shells of the studied animals exhibited growth bands, which spanned normal to the growth direction. Compression test samples were cut to rectangular prisms of approximately $6.6 \times 6.6 \times 10$ mm, in different orientations with respect to the shell layers. A load frame was used for quasi-static testing, whereas dynamic testing utilized a momentum-trapped split Hopkinson bar with pulse-shaping [see e.g. Ref. 25]. Strain rates in dynamic tests were between 200 and 500 s^{-1} . The directions of loading with respect to growth plane directions are presented in Fig. 7.

3.1.2. Bending

Samples were tested in three-point bending in various loading directions for all three shells. A high-speed diamond saw was used to section samples with a minimum length of 40 mm and cross-sectional areas of approximately 5×5 mm. Great care was taken to obtain parallel sides and uniform orientation of growth planes throughout samples. Loading orientations of the bending samples and bending stresses are presented in Table 1.

3.2. Analysis

When performing mechanical tests on natural materials such as mollusk shells, scatter in the experimental results is expected due to natural variations in microstructure and defects. Irregularities may include shell thickness, micro and macrocracks, invasion by burrowing organisms, curvature and variation in growth layers, cracks introduced by sample preparation, and structural differences due to location within the shell. Thus, it is necessary to use a statistical analysis to quantitatively evaluate the mechanical properties of these mollusk shells. While the Weibull distribution is usually used for flexural strengths, here it is used to assess a variety of quasi-static and dynamic compression data. The Weibull analysis [26] was applied by means of the equation:

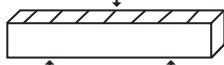


$$F(V) = 1 - \exp \left[- \left(\frac{\sigma}{\sigma_0} \right)^m \right]$$

$F(V)$ is the failure probability, m is the Weibull modulus and σ_0 is the characteristic strength; σ_0 and m are experimentally obtained parameters. The Weibull curve yields an S-shaped distribution from which the failure probability at a certain stress can be computed.

4. Mechanical properties

In all shells tested, there was a considerable dependence of the mechanical response on the direction of loading. Thus, Weibull plots for each shell under specific loading conditions show two distinct curves. These curves correspond to compression perpendicular and parallel to the direction of the growth bands. In both the abalone and giant clam shells,

Table 1
Flexure strength for various shells

Species	parallel direction, outer surface perpendicular to loading direction  Average bending stress (MPa)	layered structure perpendicular to loading direction  Average bending stress (MPa)	layered structure parallel to loading direction  Average bending stress (MPa)
Conch	74	29	x
Giant clam (outer region)	39.9	79.6	x
Giant clam (inner region)	x	7.86	x
Red abalone	x	197	177

it is observed that the compression strength of the material is greater in the perpendicular direction, yet the conch shell exhibits greater compressive strength parallel to the growth bands. This may be attributed to the tessellated “zigzag” pattern of the conch shell in which the direction of growth bands is not constant, creating a more isotropic microstructure and response.

4.1. Compression

Fig. 8(a–c) present the Weibull statistical analysis of conch, giant clam, and red abalone shell in quasi-static compression, respectively. For the conch shell, the failure probability of 50% [$F(V)=0.5$] is reached at 166 and 218 MPa for the perpendicular and parallel direction of loading, respectively. This is approximately twice the compressive strength of the giant clam shell which showed 50% failure probability at 87 and 123 MPa for loading parallel and perpendicular to layered structures, respectively. The abalone shell outperformed both the conch and the giant clam shell by over twice the compressive strength in quasi-static loading.

With failure probabilities of 50% being reached at 235 and 540 MPa with loading parallel and perpendicular to layered structure, respectively, the abalone also exhibits the highest difference in strength between loading directions, consistent with the level of microstructure anisotropy.

Dynamic compression results for the conch, giant clam, and red abalone shells are presented in Fig. 9(a–c), respectively. A similar trend in dynamic compression strength is observed with the compressive strength of abalone approximately twice that of the conch shell and the conch shell having approximately twice the compressive strength of the giant clam shell. The 50% failure probabilities of the conch shell are found at 249 and 361 MPa in dynamic loading perpendicular and parallel to layered structure, respectively. The 50% failure probabilities of giant clam in dynamic compression are found at 154 and 202 MPa for parallel and perpendicular loading directions, respectively. As in quasi-static loading, the compressive strength of the abalone shell is superior in comparison to the conch and giant clam under dynamic loading. 50% failure probabilities for the abalone shell are found at 548 and 735 MPa with the

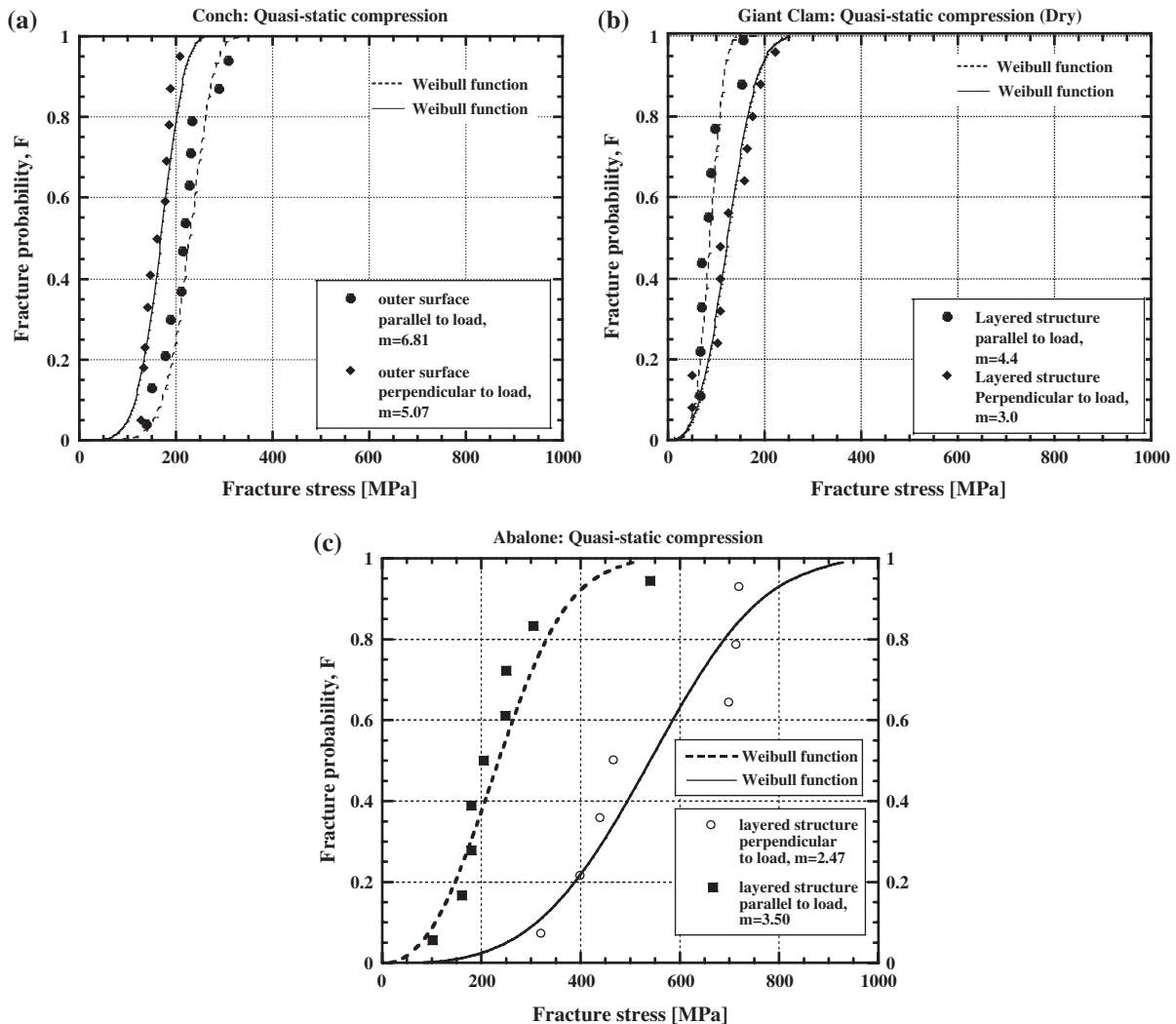


Fig. 8. Weibull analysis of: (a) *S. gigas*, (b) *T. gigas*, and (c) *H. rufescens* shells in quasi-static compressive loading.

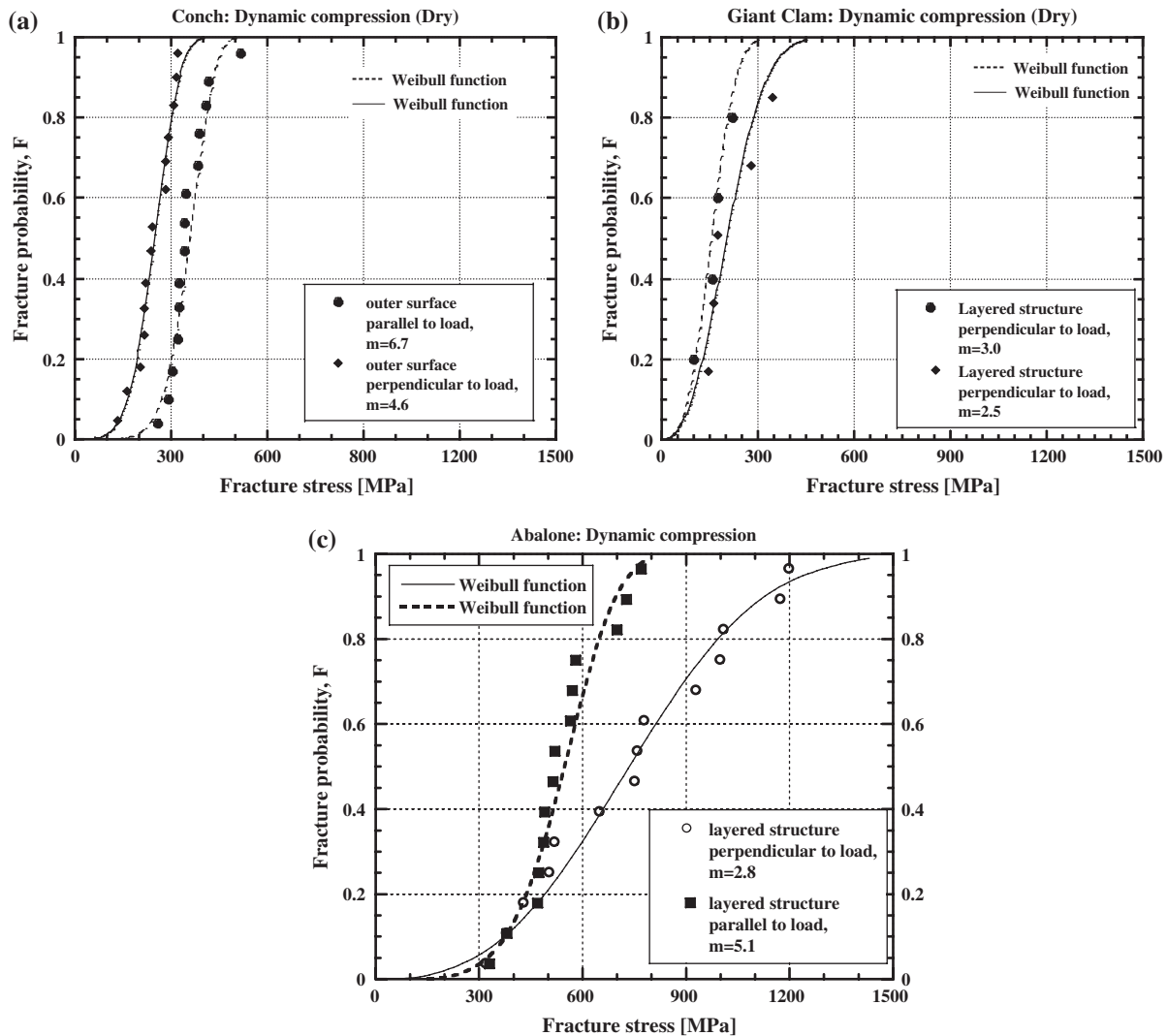


Fig. 9. Weibull analysis of: (a) *S. gigas*, (b) *T. gigas*, and (c) *H. rufescens* shells in dynamic compressive loading.

layered structure parallel and perpendicular to loading, respectively. It is clear that the materials all experience greater compressive strengths in dynamic loading than in quasi-static loading; these results have been listed in Table 2.

4.2. Three-point bending

As in compression, the abalone shell is found to have the highest bending strength of the three shells. Surprisingly, the outer, white region of the giant clam shell slightly out-

performed the conch shell. The loading direction dependency of the conch shell, with respect to its bending strength, has large variations due to the tessellated “zigzag” pattern of the conch shell, in which the direction of growth bands is not immediately obvious and could be taken in either direction.

5. Characterization of damage

5.1. Conch shell

In most brittle materials under compressive loading, failure tends to occur as a result of an axial splitting mechanism, in which fracture occurs parallel to the loading direction (e.g. [23]), and the conch shell tested here fails in a similar manner. Through the middle macro-layer (described in Section 2.1), crack propagation is blunted along the organic–inorganic interface before traveling through second-order lamellae [13]. Fig. 10 presents the resulting zigzag pattern created during failure. In this mode of failure, cracks are bifurcated and delocalized, increasing the toughness of the material.

Table 2
Comparison of compressive strengths at 50% failure probability for various shells

Species	50% failure probability stress (quasi-static loading)		50% failure probability stress (dynamic loading)	
	Perpendicular (MPa)	Parallel (MPa)	Perpendicular (MPa)	Parallel (MPa)
Conch	166	218	249	361
Giant clam	123	87	202	154
Red abalone	540	235	735	548

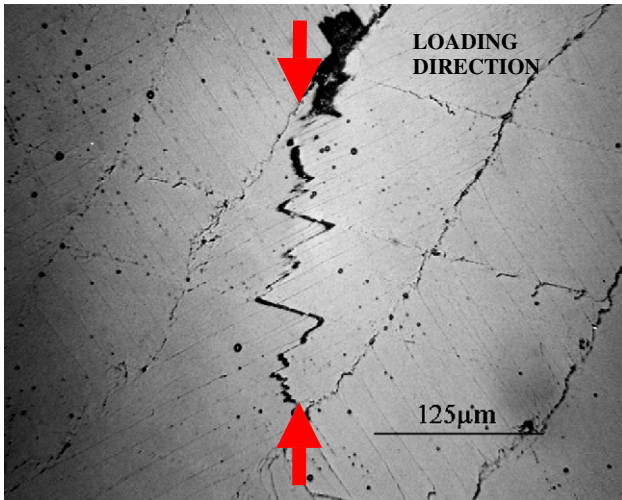


Fig. 10. Crack propagation through middle section of *S. gigas* creating a zigzag pattern through second- and third-order lamella [4].

Fig. 11 shows scanning electron micrographs of the fracture surface of the conch shell: (a) parallel to the direction of growth and (b) perpendicular to the direction of growth. The second- and third-order lamellae of the shell structure and its cross-laminar structure of alternating directionality are shown in Fig. 11(a). Separation of the lamellae at both levels is observed as fracture travels along second-order lamella wandering between third-order lamellae aragonite crystal. This failure mechanism creates a step-like fracture described by Menig et al. [13], in which third-order lamellae fracture surfaces resemble the fibrous surface of broken wood.

The fracture surface of a sample under tension (created through bending) along the axis of shell growth is shown in Fig. 11(b). Separation along this axis exposes all three orders of lamellae as described in Fig. 1. Planes of aragonite tablets in alternating orientation comprise the second order lamellae. The conch shell structure achieves its toughness through its hierarchical lamellae microstructure, in which single crack tips are delocalized by a large number of smaller cracks over a broader region, alternating direction at each lamellar level.

5.2. Giant clam shell

The microstructure of the *T. gigas* (giant clam) shell was described in Section 2.2. It consists of both an inner, translucent brittle region, with relatively low organization, and an outer white, tougher region, which resembles the shell of the *S. gigas* (conch). The inner region fails at the crystal interfaces seen in Fig. 4 through a mechanism of axial splitting. Initial microcracks within this region extend and coalesce under applied stress, resulting in the failure of the shell samples.

The material suffers in mechanical strength as a result of these flaws, resulting in weak properties in comparison to other shells, such as conch and abalone [13,18]. It is important to note that the mechanical strength of the outer solid white region of the clam shell is over ten times that of the inner

translucent region. Fig. 12 shows scanning electron microscopy of the fracture surfaces of the shell in bending (a) perpendicular to growth bands and (b) parallel to growth bands; this directional dependency has been further clarified in Table 1. A cross-lamellar structure can be seen in Fig. 12(a), in which the horizontal line marked with an arrow is a growth band extending perpendicular to the fracture surface. The alternating planes of fibrous crystals travel at 30° angles to the planes of the growth bands. Separation of material at the growth band interfaces occurred in shear during bending loading perpendicular to planes of growth interruption. Fig. 12(b) shows the fracture surface of a sample under tension in bending. Separation occurred across a single growth band and second-order lamellae are observed as planes of fibers traveling perpendicular to the fracture surface and alternating in fiber angles. The surface separated cleanly at a single growth band across the entire sample. These observations indicate that separation occurs at the growth band interfaces in both loading directions, parallel and perpendicular to the growth direction.

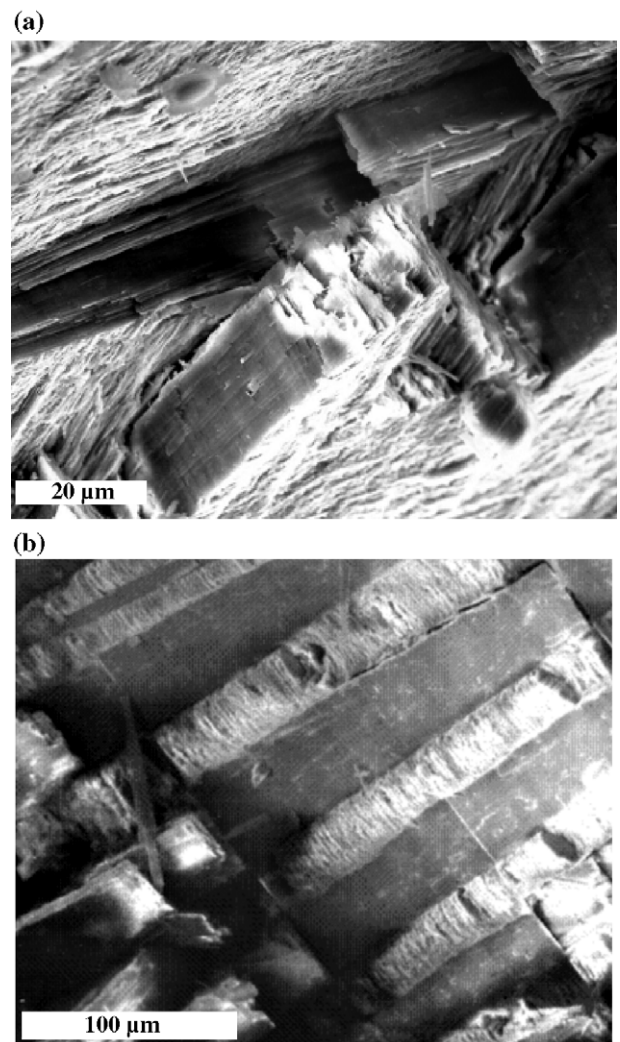


Fig. 11. Fracture surface of *S. gigas* (a) parallel to growth direction and (b) perpendicular to growth direction.

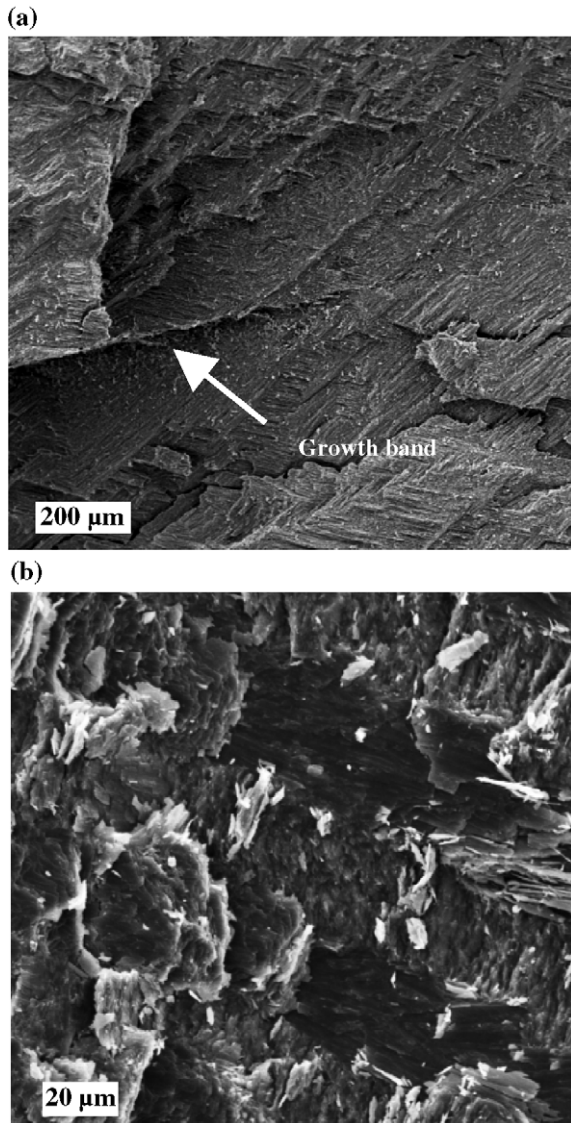


Fig. 12. Fracture surface of *T. gigas* under bending (a) perpendicular to growth bands and (b) parallel to growth bands.

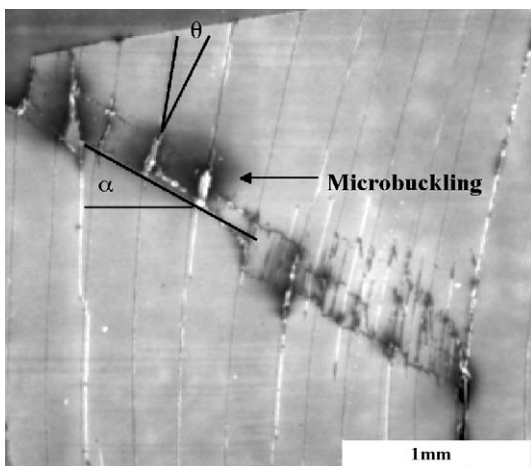


Fig. 13. Microbuckling observed at mesolayers in *H. rufescens* shell under compressive loading.

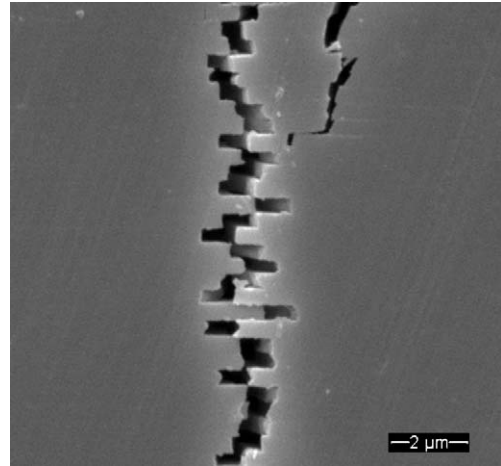


Fig. 14. Toughening mechanism of tile pullout in *H. rufescens* nacre during tensile fracture.

5.3. Red abalone shell

In the nacre of the red abalone, both the macro- and microstructure of the shell resemble the structure of other manmade laminate composites [e.g. Ref. 27]. As described in Section 2.3, the macrostructure is characterized by mesolayers, which separate larger regions of nacre. These mesolayers, composed of organic material, act as a softer viscoelastic layer separating more ridged sections of brick-and-mortar-like nacre. The result is a structure similar to fiber-reinforced composites, in which phenomena such as plastic microbuckling can be observed. Fig. 13 shows plastic microbuckling occurring at mesolayers, decreasing overall strain energy, when loading is parallel to the layers. This mechanism of failure is common in fiber-reinforced composites and has been well studied in other synthetic materials [28–33].

Examining the failure at a scale below that of the mesolayers, we see a tortuous path of crack deflection through micro-layers of hexagonal tiles of aragonite [1]. These tiles, as described in Section 2.3, form a brick-and-mortar-like structure resulting in further mechanisms of toughening [11,12]. Fig. 14 shows sliding of tiles under tension parallel to the tile planes. In most cases, the tiles slide apart at the organic interfaces rather than fracturing through the aragonite crystals. This failure mode creates a mechanism of toughening identified and described by Sarikaya [1] and Evans et al. [34]. The tensile strength of the ceramic is estimated to be at least four times the shear strength of the organic layer [20].

6. Conclusions

These shells are the primary means of protection for the soft bodies of mollusks. They provide these animals with a permanent encasement of body armor, which must be strong enough to withstand the impact and compression capabilities of a sea of predators. From the observations and analysis within this study, it is clear that the micro- and macrostructure of these shells plays a significant role in increasing the

toughness of an otherwise brittle base material, CaCO_3 . In each shell, the viscoplastic deformation of the organic interfaces and the crack delocalization due to the layered microstructure of the inorganic aragonite lead to an increase in mechanical strength of the biocomposite above its base monolithic aragonite. From the three shells in this investigation, it was neither the most organized structure (conch shell) nor the least organized structure (inner section of giant clam shell) that exhibited the greatest mechanical strength but rather the abalone, with its optimized hierarchically organized brick-and-mortar system. The abalone exhibited a compressive strength approximately twice that of conch shell and four times that of the giant clam shell, when loaded either quasi-statically or dynamically. The inner section of the giant clam is an order of magnitude weaker than the outer section of the same shell due to differences in microstructure. A strong dependence on loading direction with respect to microstructure was observed in all of these shells. It can be concluded that the microstructure of these biological materials determines the mechanical properties of each shell, with structures having an over-organized, under-organized, or optimized hierarchy.

Acknowledgements

We would like to thank Evelyn York at the Scripps Institute of Oceanography for her assistance with scanning electron microscopy. Dr. David Leighton of Marine Bioculture provided us with abalone specimens and valuable consultation. We would also like to thank Professor Sarikaya (University of Washington) for insightful discussions and inspirations. Rex Graham was instrumental in giving this work greater exposure.

References

- [1] M. Sarikaya, *Microsc. Res. Tech.* 27 (1994) 360.
- [2] A.V. Srinivasan, G.K. Haritos, F.L. Hedberg, *Appl. Mech. Rev.* 44 (1991) 463.
- [3] J.F.V. Vincent, *Structural Biomaterials*, Princeton Univ. Press, Princeton, NJ, 1991.
- [4] L.F. Kuhn-Spearing, H. Kessler, E. Chateau, R. Ballarin, A.H. Heuer, *J. Mater. Sci.* 31 (1996) 6583.
- [5] S. Weiner, H.D. Wagner, *Annu. Rev. Mater. Sci.* 28 (1998) 271.
- [6] S. Weiner, L. Addadi, *J. Mater. Chem.* 7 (1997) 689.
- [7] E. Baer, A. Hiltner, R.J. Morgan, *Phys. Today* (1992 (Oct.)) 60.
- [8] H.A. Lowenstam, S. Weiner, *On Biomineralisation*, Oxford Univ. Press, New York, 1989.
- [9] G. Nicolis, I. Prigogine, *Self-Organization and Nonequilibrium Thermodynamics: From Dissipative Structures in Order through Fluctuations*, Wiley, New York, 1997.
- [10] G. Whitesides, *Mater. Res. Bull. Jpn.* (2002) 56.
- [11] M. Sarikaya, J.A. Aksay, in: S. Case (Ed.), *Results and Problems in Cell Differentiation in Biopolymers*, Springer-Verlag, Amsterdam, 1992, p. 1.
- [12] M. Sarikaya, K.E. Gunnison, M. Yasrebi, J.A. Aksay, *Mater. Res. Soc.* 174 (1990) 109.
- [13] R. Menig, M.H. Meyers, M.A. Meyers, K.S. Vecchio, *Mater. Sci. Eng., A Struct. Mater.: Prop. Microstruct. Process.*, 297 (2001) 203.
- [14] S. Weiner, *Am. Zool.* 24 (4) (1984) 945.
- [15] J.R. Rosewater, *Indo-Pac. Mollusca* 1 (1965) 347.
- [16] B.G. Moir, *J. Archaeol. Sci.* 17 (1990) 329.
- [17] I. Kobayashim, *Am. Zool.* 9 (1969) 633.
- [18] R. Menig, M.H. Meyers, M.A. Meyers, K.S. Vecchio, *Acta Mater.* 48 (2000) 2383.
- [19] J.D. Currey, *J. Zool. London* 180 (1976) 445.
- [20] A. Lin, M.A. Meyers, *Mater. Sci. Eng., A Struct. Mater.: Prop. Microstruct. Process.* 390 (2005) 27.
- [21] C.M. Zarella, A.M. Belcher, M. Fritz, Y. Li, S. Mann, P.K. Hansma, D.E. Morse, *Chem. Mater.* 8 (1996) 679.
- [22] X. Su, A.M. Belcher, C.M. Zarella, D.E. Morse, G.D. Stucky, A.H. Heuer, *Chem. Mater.* 14 (2002) 3106.
- [23] M.A. Meyers, K.K. Chawla, *Mechanical Behavior of Materials*, Prentice-Hall, Upper Saddle River, NJ, 1999, p. 41.
- [24] A.P. Jackson, J.F.V. Vincent, R.M. Turner, *Proc. R. Soc. Lond., B* 234 (1988) 415.
- [25] G.T. Gray, *Classical Split Hopkinson Pressure Bar Testing*, ASM Handbook, vol. 8, 2000, p. 462.
- [26] W. Weibull, *Ingenioersvetenskapsakad. Handl.* 1 (1939) 151.
- [27] D.J. Harach, K.S. Vecchio, *Metall. Mater. Trans.* 32A (2001) 1493.
- [28] A.S. Argon, *Treatise of Materials Science and Technology*, Acad. Press, New York, 1982, p. 79.
- [29] B. Budiansky, *Comput. Struct.* 16 (1983) 3.
- [30] A.G. Evans, W.F. Adler, *Acta Metall.* 26 (1997) 725.
- [31] N.A. Fleck, L. Deng, B. Budiansky, *J. Appl. Mech.* 62 (1995) 329.
- [32] P.M. Jelf, N.A. Fleck, *J. Comput. Mater.* 26 (1992) 2701.
- [33] M. Dao, R.J. Asaro, *Scr. Mater.* 34 (1996) 1771.
- [34] A.G. Evans, Z. Suo, R.Z. Wang, I.A. Aksay, M.Y. He, J.W. Hutchinson, *J. Mater. Res. Soc.* 16 (2001) 2475.